MICROCOPY RESOLUTION TEST CHART
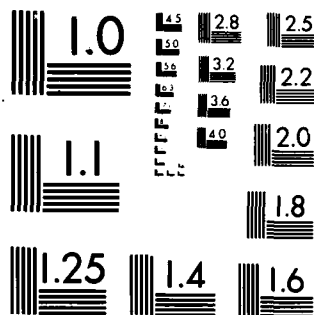NATIONAL BUREAU OF STANDARDS-1963-A

ELECTRONIC STRUCTURE OF INTERFACE
STATES OF MOS AND SOS DEVICE MATERIALS

By

AD-A173 905

PROFESSOR B. HENDERSON

Department of Physics
University of Strathclyde
John Anderson Building
107 Rottenrow
Glasgow G4 ONG
Scotland

CONTRACT DAJA 45-83-C-0049

DTIC
ELECTE
NOV 7 1986
S
A

FINAL TECHNICAL REPORT

24 April 1986 - 23 August 1986

This document has been approved
for public release and sale; its
distribution is unlimited.

OTIC FILE COPY

86 11 7 001

A. Research Programme 1984-1986

The current success of the Si semiconductor technology arises from the surface passivation afforded by the native oxide SiO_2. This oxide layer, normally produced by thermal oxidation of Si, does not bond to the substrate without some broken bonds being left at the interface. Fortunately the density of defect states is low. Being assoicated with broken bonds these defects produce a fixed charge at the interface. EPR signals arising from defects at the Si/SiO_2 interface were first observed by Nishi.[1] The identification and characterisation of the defects as electrons in broken sp^3 bond pointing into the interface owed much to the pioneering work of Poindexter and his colleagues at ETDL, Fort Monmouth.[2] The centres were labelled P_B in $\langle 111 \rangle$ wafers. The spectrum from $\langle 100 \rangle$ wafers was observed to have two components, labelled P_{B0}, P_{B1}. The P_{B0} centre was found to be identical to the P_B signal in $\langle 111 \rangle$ wafers i.e. coming from a dangling bond on an interfacial silicon atom. The difference in the g-tensors was explained as being due to the different orientation of the dangling bond in $\langle 111 \rangle$ and $\langle 100 \rangle$ wafers. The second $\langle 100 \rangle$ centre, P_{B1} was assigned to the species, $Si \equiv Si_2O$ at the interface. Lenehan et al.[3] have shown that exposure to gamma rays can cause a dramatic increase in P_B concentration in $\langle 111 \rangle$ wafers. It can be supposed that the passage of ions through the interface would have a similar effect. This work by the ETDL group showed there to be a quantitative relationship between the P_b centre concentration and the amount of fixed charge at the interface. Subsequent ESR work by Brower[4], which resolved the ^{29}Si hfs, proved that this $s = \frac{1}{2}$ spectrum fitted Poindexter's model. Assuming a freshly cleaved Si surface there are some 10^{14} atoms cm^{-2}: if 10% of the bonds are unused in bonding following thermal oxidation then there are ca $10^{13} cm^{-2}$ broken bonds. Since

the typical ESR sensitivity is 10^{13} centres/mT linewidth it is clear that the ESR measurements must be made close to the sensitivity limit. Much of the present study aimed at with improving the sensitivity of the ESR phenomenon by measuring spin dependent changes in such physical properties as DLTS, photoluminescence and photoconductivity. These measurements also addressed fundamental questions about the Si/SiO_2 interface e.g. where do the energy levels of the P_b centre occur in the gap? Is the P_b centre light sensitive and does the P_b centre act as a recombination centre. The second part of the work concerns the nature of the radiation damage due to P^+ ion implantation, paying particular attention to the ion energy dependence of the defect production rate and the thermal stability.

The use of ion implantation in silicon device fabrication is known to give rise to defects both in the silicon and oxide. Some of these defects may be capable of withstanding even high temperature ($1000°C$) anneals. Renewed interest in ion implantation in Si/SiO_2 device structures in recent years has led to the use of a variety of experimental techniques to investigate the nature of damage produced by implantation of ions in the energy and dose ranges of technological interest. Since such defects may be paramagnetic, EPR has proved to be a very useful technique for studying radiation damage on an atomic scale. Ion irradiation of amorphous SiO_2 produces two predominant paramagnetic centres, one associated with an oxygen vacancy (E'_1) and the other with a non-bridging oxygen atom (oxygen hole centre). There is a marked difference between the EPR spectra of these centres. The E'_1 centre is characterised by an almost axial g-tensor which in thermal oxides gives rise to a glassy lineshape with apparent g-value of 2.0005 and linewidth of $\simeq 2G$ (at X-band). The ESR signal saturates at low levels of microwave power. The OHC also exhibits a glass

lineshape but the spread of g-values is much larger giving rise to a very extended spectrum.

B. <u>Sources of Si/SiO$_2$ materials and characterization</u>

All samples used in the present studies were obtained from the GEC Research Laboratories, Hirst Research Centre, Wembley UK. They were <100> or <111> orientated wafers of vacuum float-zone melted silicon with rather small p-type conductivity (4 - 20 $(\Omega cm)^{-1}$): These wafers were cut from 3" or 4" diameter boules and were of 0.03 - 0.04 ins. thickness. A thin layer (30μm) of amorphous Si was then deposited on one surface. The other surface was thermally oxidised by heating in flowing moist oxygen at 700 - 1000$^{\cdot}$K for 30 - 60 minutes. The oxide thickness varied in from 50 - 100 nm.

Characterisation of these materials was by electron spin resonance (ESR) spectroscopy. Samples of approximate area 1.5 x 0.5 cm^2 were cleaved from the 3" or 4" diameter discs and the ESR spectrum recorded using a Varian 4502 ESR spectrometer operating at 9.5 GHz or 77 K. Typical spectra consisted of several partially overlapping lines; although the relative intensities were quite small, large variations were observed between samples. Always present were resonances from E_1' centres in the amorphous SiO$_2$, P_b centres at the interface, P and Fe in the bulk Si and surface dangling bond resonances introduced during cleavage of the wafer. The E_1' centre signal saturates very easily as a function of microwave power (typically 10 mW is sufficient to cause complete saturation). Surface centres introduced by cleaving had a g-value of 2.0085. This was established by etching off the sample edges. After this treatment the

intensity of ESR spectra was fairly consistent from one sample to another. For example the P_b centre concentration was <u>ca</u> $(5\pm1) \times 10^{10}$ cm^{-3}. We developed the following procedure to establish the origin of the resonances:-

(i) *Record the ESR spectrum at low microwave power to maximise the E_1' centre signal.*

(ii) *Record the ESR spectrum at high microwave power to the E_1' centre resonance and optimize other resonances.*

(iii) *Mask the oxide region and etch off the sample edges.*

(iv) *Remove the oxide and polysilicon layers by etching to distinguish between bulk Si and interface/oxide paramagnetic centres.*

A typical spectrum is from a sample from which the SiO_2 layer was removed shown in Fig. 1(a): there are two lines the P_{am} line and the P donor resonances at g = 1.999. After etching away the amorphous Si layer there is no P_{am} resonance left, so that only the g = 1.999 resonance can be detected. Normally after cleaving the sample we would go immediately to stage 3, once the general features of particular material had been established.

C. Experimental results and discussion

(i) Spin dependent photoconductivity (SDP) and optically induced ESR

The strength of the P_b centre ESR signal is strongly enhanced by white light is some samples, and is extremely sensitive to microwave power. Saturation of the ESR sets in at much lower microwave power levels (0.7 mW) in the absence of light than under the conditions of optical pumping. The ESR intensity sturates when the spin flip probability (γB_1) is equal to the

relaxation rate T_1^{-1}. The (dark) ESR signal saturates at $\sim$ 0.7 mW, corresponding to a spin-lattice relaxation time $T_1 \simeq 10^{-5}$s. However, in the presence of optical photons one observes saturation at much higher microwave power levels ($\simeq$ 100 mW). The corresponding relaxation time is of order $T_1 \simeq 10^{-7}$s. The difference in relaxation time reflects the fact that it is the total lifetime due to both T_1 and other processes which determines the saturation behaviour. These "other processes" are of course light induced and include the timescale of the optical pumping cycle. Indeed simply summing the relaxation rates for spin lattice (T_1) and other processes (T_0) gives $T^{-1} = T_1^{-1} + T_0^{-1}$. Noting the total lifetime differs by more than an order of magnitude from the ESR (dark) values leads to the conclusion that it is the optical processes which dominate the relaxation behaviour for light-induced ESR. The spin dependent photoconductive (SDP) resonance has been remeasured at 24 GHz and at T = 1.6 K.[5] The spectra were recorded with the static magnetic field, B parallel to the (111) surface of the crystal. To improve the signal/noise ration the spectrum was signal averaged for 100 sweeps. Figure 1(a) also shows the spin-dependent photoconductive resonance (SDPR) signal at 4.2 K using 100 mW of microwave power. Note that the sign of this signal is negative, corresponding to a decrease in the photocurrent. That this is the case demonstrates in a single spectroscopic experiment that the P_b centre levels act both as a recombination centres and interface states in Si/SiO_2. Band gap light excites electrons from the valence band into the conduction band: such transitions are spin conserving (i.e. $\Delta S = 0$). Electrons in the conduction band may then recombine with the dangling bond defect either directly or indirectly via some nearby trap with energy close to the conduction-band edge. Recombination proceeds preferentially via spin conserving processes, i.e. between centres whose spins are aligned

antiparallel with respect to each other. There is a 3:1 probability, however that a spin triplet state is formed from which recombination transitions are only weakly allowed. Hence, there is a build-up of population for such centres. Microwaves at the resonance frequency change the spin orientation of either the electron or the dangling bond so enhancing the relative concentration of S = 0 centres. In consequence, the number of operative recombination channels is increased and the photocurrent decreases. The sensitivity of the technique depends upon the non-Boltzmann-like distribution of the spin system. In thermal equilibrium the intensity of the SDPR resonance intensity should follow the spin polarization; hence, $\Delta P/P \approx 10^{-6}$ at room temperature.

The detected changes in photocurrent are of order 10^{-4}. Since we have not measured the luminescence it is not clear whether recombination proceeds radiatively or nonradiatively. However, both centres involved in the recombination process should undergo microwave driven spin-flip transitions and so both resonances should be observed. We observe a single line spectrum, at the g-value of the P_b centre, with weak hfs due to the $I = \frac{1}{2}$ nucleus ^{29}Si. The additional spurious line can be removed by etching away the sample edges to remove surface centres introduced by cleaving the sample.

(ii) Photoluminescence (PL) and optically detected magnetic resonance (ODMR)

The P_B centre SDP signal is observed by using bandgap radiation ($h\nu \sim$ 1.2 eV) to photoexcite carriers into the conduction and valence bands. This same process leads to rather weak recombination luminescence (Figure

2(c)). The ESR signal may also be measured with enhanced sensitivity by recording the changes in intensity of the circularly polarized emission from Si/SiO$_2$ samples in a magnetic field, induced by resonant microwave radiation (Figure 2(b)). Using this ODMR technique an ESR signal is recorded at the same g-value as the P$_b$ centre resonance to be which is identical with that seen in the SDP experiment. The spectra are compared in Figure 2. The SDP and ODMR results show that the P$_b$ centre acts as a centre for radiative and non-radiative recombination.

In samples excited through the thick oxide layer with 337 nm radiation from a Kr$^+$ laser we have observed resonances due to spin triplet states in the amorphous SiO$_2$. In the first measurements made at 24 GHz the Si/SiO$_2$ sample was of typical dimensions 5mm x 2mm x 35μm. The sample was placed at the centre of a cylindrical TEO11 cavity, submerged in liquid He at the centre of a 5T superconducting solenoid. Figure 3 shows the wavelength dependence of the blue emission from the SiO$_2$ surface, excited either using the 337 nm radiation or 50 KV X-rays. For comparison the X-ray excited luminescence from pure SiO$_2$ is also plotted (after Hayes et al. 1984). Figure 4 plots the microwave induced change in the total emission intensity as a function of magnetic field, detected through a blue edge filter. There are at least five, (rather) broad resonance peaks. The relative magnitude of the signal is about 1% of the overall light level, showing that the ODMR effect is determined not by a Boltzmann distribution of the triplet spin states but by the selection rules ($\Delta M_s = \pm1$). In consequence the radiative lifetime $\tau_R < T_1$, where T_1 is the spin-lattice relaxation time. The ODMR spectrum in Figure 4 increases in intensity with the square of the laser power. Thus the exciton luminescence must arise from two-photon absorption.

Also shown in Figure 4 are the major extrema in the ODMR spectrum of trapped excitons in single crystal quartz (after Hayes et al. 1984). The triplet exciton spectrum has een reported by Hayes et al. at Oxford University in single crystal quartz uder X-ray treatment. In the present case we observe only the polycrystalline average of the single crystal spectrum. Hence one sees only vestiges of the signal a the turning points of the orientation dependence of the single crystal pattern.

The obvious similarities between the luminescence and ODMR spectra of the SiO_2 layer and single crystal quartz suggests that the same defect is being produced in both instances. Hayes et al. (1984) interpreted their spectra in terms of the formation of trapped excitons, and we are tempted to draw the same conclusion here. To test this we have simulated the powder spectrum using the orientationally averaged spectrum of the single crystal data for excitons in SiO_2. The spin Hamiltonian for an $S = 1$ centre in orthorhombic symmetry is given by

$$H = \mu_B \, \underline{S} \cdot \tilde{\underline{g}} \cdot \underline{B} + D\left[S_z^2 - 1/3S(S+1)\right] + E\left[S_x^2 - S_y^2\right] \tag{1}$$

In high magnetic field such that $g\mu_B B \gg D,E$ solutions of eqn (1) give the two $M_S \rightarrow M_S + 1$ resonance fields transitions to first order as

$$B = B_0 + \tfrac{1}{2}(2M+1)[D(3\cos^2\theta-1) + 3E\cos2\Phi(1-\cos^2\theta)] \tag{2}$$

where θ and Φ are the usual polar angles and the g-value g is assumed to be isotropic. In a powder sample, and to a good approximation the amorphous oxide layer is just that, defects are randomly orientated with respect to the magnetic field direction. Therefore we have assumed a perfectly random array of excitons in these materials. Hence all centres with axes between

(θ,Φ) and ($\theta-d\theta,\Phi+d\Phi$) contribute to the spectrum at the resonance field B(θ,Φ), with intensity determined by the lineshape $D_i(\theta,\Phi)$, where i refers to the particular transition. Thus the total intensity at B(θ,Φ) is just

$$I(B) = \sum_i \int D_i(\theta'-\theta, \Phi'-\Phi) \, dn(\theta',\Phi') \qquad (3)$$

where $dn(\theta',\Phi')$ is the number of centres in the solid angle $d\Omega = d\Phi d(\cos\theta)$ = $(4\pi/N)dn(\theta',\Phi')$, $D_i(\theta,\Phi)$ is the lineshape function and N is the total number of centres. Hence the shape of the spectrum depends on

$$\frac{dn}{dB} = \frac{dn}{d\Omega} \cdot \frac{d\Omega}{dB} \qquad (4)$$

To obtain I(B), or more precisely the maxima in I(B) for a triplet state in orthorhombic symmetry the solution of eqn (1) gives a sixth order equation. In consequencehence six peaks are to be expected (neglecting g-tensor anisotropy), which taken in pairs have separations given by 2D, D+3|E| and D-3|E|. Obviously the spectrum does not give such a symmetrical distributions of lines, presumably because g- is anisotropic and because the selection rules for ODMR are also strongly anisotropic. This is precisely what is observed in the 35 GHz spectrum (Figure 5). That this simple spectrum is not observed at 24 GHz (Figure 4) arises from the fact that Ka-band photon is not sufficiently energetic to excite all possible $\Delta M_s = \pm1$ transitions. From the measured Q-band spectrum (Figure 5) we determine g_z = 2.001 ± 0.005, g_x = 2.020 ± 0.01, g_y = 2.015 ± 0.005, D = 903 ± 5 mT and E = 35 ± 7 mT, spin Hamiltonian parameters which are in excellent accord with those of the trapped excitons in single crystal SiO_2. This analysis shows the advantage of working at the higher microwave frequency since all six resonance transitions are excited. In addition corrections of order D^2/B_0 and E^2/B_0 are somewhat smaller, having the effect of sharpening up the transitions and making the spectrum appear

rather more symmetric. We have not calculated selection rules for emission of circularly polarised radiation: These are strongly dependent upon the interplay of radiative and non-radiative de-excitation, which in are turn dependent on orientation of the defect axes relative to the fixed magnetic field.

(iii) Ion implantation

Radiation damage is well characterised in both Si and SiO_2 and it is natural to extend such studies to device materials based on Si/SiO_2 wafers. The ultimate aspiration is to give strong guidance in the design of radiation-hard device structures. The nature of the damage that occurs in silicon during ion implantation depends on such parameters as ion mass and energy, dose and substrate temperature. At low doses the creation of point defects predominates. With increasing dose the formation of amorphous regions or continuous amorphous layers occurs. Crowder et al. studied the effect of phosphorous ions in silicon by monitoring the g = 2.0055 line which is a charauteristic EPR signal in amorphous silicon. They found that the signal increased linearly with dose initially (up to a dose of ~ 5 x $10^{14}cm^{-2}$). This was followed by a second linear region with much lower slope. The initial linear increase was interpreted as being due to the formation of localised amorphous regions. The precise mechanism of amorphous layer formation is, however, still not certain. A more complicated picture arises when the implantation is performed through an oxide layer. Here it may be necessary to consider the effects of recoiling atoms from the SiO_2.

To date we have only worked with $\langle 111 \rangle$ Si/SiO$_2$ wafers implanted with the spectroscopically inactive ion phosphorous. The samples were n-type with a resistivity of 25 Ωcm. All implantations were carried out through the oxide layer, with doses varying from 10^{12} - 10^{15}e cm^{-2} and energies of 20, 30, 45 and 120 keV. The ion energies were chosen so that the implanted ion comes to rest (i) mainly in the oxide layer, (ii) mainly at the interface, and (iii) mainly in the Si. The particular ion energies were 20 keV, 30 keV, 45 keV and 120 keV which have calculated peak ranges R$_p$ and distribution half-widths Γ of:-

	R$_p$(nm)	Γ(nm)	% Ions in SiO$_2$
20	24	13	98%
30	32	18	30%
45	52	25	50%
120	143	58	6%

The numbers in the last column refer to that percentage of implanted ions which come to rest in an oxide layer of thickness 51 nm: apparently at 45 keV the peak in the distribution of P$^+$ ranges in the Si/SiO$_2$ wafer is at the interface between silicon and the native oxide. Implantation doses ranged from 10^{11} - 10^{16} ions cm^{-2}. In this report we concentrate on ESR studies in which we have determined the concentrations of the E$_1'$ centres in the oxide and the amorphous centre in silicon. We will label the latter P$_{am}$ and note that it includes the simple amorphous centre and the oxygen associated centre. Since all of the centres observed overlap to some degree concentrations are determined by fitting to a computer generated spectrum.

The major effect of low energy ($<$ 25 keV) implantation was the creation of E_i' centres and both 'wet' and 'dry' hole centres (ratio 1:2) in overall concentrations independent of pre-irradiation annealing treatment. Few defects are created in the thermal oxide. At the highest dose levels E_i' centrespin concentrations of order $10^{14} cm^{-2}$ were recorded corresponding to total concentration of order $10^{19} cm^{-3}$. By etching off successive layers of SiO_2 it was established that the peak in E_i' centre concentration occurred at approximately half the depth of the thermal oxide. At intermediate electron energies ca 45 keV, the peak in the damage distribution should occur at the interface. In 'as-implanted' wafers the predominant effect remains a very intense E_i' centre ESR signal, saturating at doses near $10^{14} e$ cm^{-2}. Successive etch removal of the SiO_2 layer reveals the P_b centre resonance once the oxide thickness has been reduced to ca 5.0 nm. The concentration of P_b centres was still relatively small. For a fluence of $5 \times 10^{13} e$ cm^{-2} the interface state defect concentration was only $5 \times 10^{12} cm^{-2}$ which is very little different from the un-irradiated material. Etching through the interface revealed a resonance due to dangling bond centres in bulk silicon at $g = 1.999$. Finally at high implant energies (120 keV) the samples should contain most P ions under the Si interface. However, as might be expected the strongest EPR signal was for E_i' centres. Etching removed these and the P_b centre and P_{am} resonances leaving mainly the $g = 1.999$ resonance noted above.

These studies indicate that (i) the principle defects produced by ion implantation are determined by ion energy: under appropriate experimental conditions one observes E_i' centres and trapped hole centres in the SiO_2, P_b centres at the interface and bulk Si_3^+ resonances in Si substrate. (ii) The concentrations vary linearly with dose, and as might be expected show an in

mass dependence also. Given that in good quality materials the P_b interface state density is only ca 5 x $10^{10} cm^{-2}$, it is evident that the concentration of P_b centres is enhanced only by a factor of ca 100.

Figure 6 show the low power spectra obtained from samples of varying doses. The E_1' line is seen to broaden and change lineshape as the dose increases. This broadening effect is caused by a spin-spin interaction between neighbouring defects at high defect densities. Plotted in Figure 7 for each implant energy are the dose dependences of E_1' centre production measured using ESR about 7 days after implantation. For each ion energy the curves are of the same general shape i.e. a dose range of linear increase followed by (almost) saturation. Note that as the ion energy increases the dose at which saturation occurs increases from 5 x 10^{13} cm^{-2} (20 keV) to 5 x 10^{14} cm^{-2}, whereas the saturation concentration increases from 2 x 10^{12} to ca 5 x 10^{13}. This would appear to be consistent with the tabulated range data since the higher the implant energy, the greater the range and the more the energy is expended in the Si rather than SiO_2 region. Our values for E_1' concentrations are about one order of magnitude lower than Devine obtained using Ar^+ ion implants. Since argon is slightly heavier than phosphorous, Devine's concentration should be higher. However, the mass correction is very small compared to the difference in saturation concentration of 4 x 10^{13} E_1'/cm^2 (Devine) and ~ 2 x 10^{12} (this work). The reason for such a large disagreement is not very clear. Concentrations obtained following 60 keV As^+ implantation of Si/SiO_2 were several orders of magnitude lower than expected, and were explained in terms of e.g. lattice heating during implantation. However, the E_1' concentration is known to be reduced by hydroxyl groups in the oxide. The presence of these groups was evidenced by observation of the wet OHC

signal. In consequence Devine's higher values for E_1' concentration would indicate that his oxides had relatively low OH content: in fact he doesn't report observing any OHC signal.

In Figure 8(a) is shown a spectrum obtained using a sample irradiated with 20 keV P^+ ions to a fluence of $5 \times 10^{15} cm^{-2}$. For samples irradiated with 20 keV P^+ we have observed a marked decay of the E_1' centre concentration time. The spectrum in Figure 8(b) was recorded some 90 days later, under exactly the same experimental conditions except for the amplifier gain setting. The E_1' centre signal has clearly narrowed, and in so doing revealed a part of the OHC spectrum. There has also been a decrease of some 60% in the concentration of E_1' centres. This effect increases for high doses: as Figure 9 shows the effect saturates at 60% decrease for doses in excess of $6 \times 10^{14} cm^{-2}$. Such a time dependent decrease in E_1' centres with dose has not previously been reported, although we note the similarity in behaviour between E_1' centres here, and F^+ centres in CaO and SiO during Na^+ implantation. In much lower dose As^+ implantation Stesmans has observed E_1' signals that are stable over many months; in such samples the concentration of E_1' centres is probably too small to be observed. Although we have no specific mechanism to explain these effects, we note that at high dose displacement spikes due to different P^+ ions are likely to overlap. In consequence there may be a slow radiation enhanced diffusion mechanism at room temperature in these overlap regions. Defect diffusion may lead to annihilation of centres i.e. decrease in E_1' centres or the creation of new centres (i.e. decrease in E_1', appearance of OHC). We have no means at this time of determining between these or other possible mechanisms. Figure 9 is a compilation of data showing the decrease in E_1' centre concentration with time (on a log-linear

scale) for the same samples as used in Figure 7. Generally it appears that
there is a sharp decrease in E_1' centre concentration immediately after
implantation, and that the rate decreases with increasing time. The effect
of increasing dose and increasing energy is to enhance this effect.
Saturation of the effect is rather faster at higher fluences and (for the
same dose) at higher ion energy.

Figure 6 shows the spectrum from a sample irradiated with 120 keV P^+
ions to a dose of $5 \times 10^{14} cm^{-2}$: the P_{am} and E_1' signal can both be seen.
The measured P_{am} concentration of $2.5 \times 10^{13} cm^{-2}$ is just less than the
saturation value. The energy loss in oxide is ~ 45 keV so the ions enter
the silicon with $E = 75$ keV. We obtain a saturation dose of $5 \times 10^{14} cm^{-2}$,
in good agreement with the expected value of $5 \times 10^{14} - 6 \times 10^{14} cm^{-2}$ for P^+
implantations. The P_{am} concentration following saturation is found to be $3
\times 10^{13} cm^{-2}$. Following 200 keV P^+ implantation of bare silicon Morehead
found a saturated P_{am} concentration of $1.4 \times 10^{15} cm^{-2}$. If we assume that
this concentration scales linearly with implant energy then we would expect
a value of $5 \times 10^{14} cm^{-2}$ for 75 keV P^+.

During ion implantation Si/SiO$_2$ samples during ion implantation emit a
relatively bright blue luminescence. This suggested that measurement of
the photoluminescence spectrum after implantation might give important
information about the nature of the defect structure of the implanted
surface. We show in Figure 2 the luminescence excited by radiation at 337
nm from an Ar^+ laser. There are three features: a broad band luminescence
centred near 402 nm, with semblances of structure that vary with samples; a
rather sharp band close to the band gap at 1.02 μm which we have shown to
be associated with P_b centres and, a band at 1.5 μm. The relative

intensities of these three bands vary with sample. However within a particular sample the bands intensities vary linearly with fluence in the range 10^{14} - 10^{16} ions cm^{-2} with energies E = 45 keV. Preliminary ODMR studies have been made of each of these bands. Very weak triplet exciton ODMR is observed on the 402 nm band: the signal is not as strong as in un-irradiated samples. This suggests that only a part of the luminescence band is associated with the formation of triplet excitons in the amorphous SiO$_2$ layer. The 1.02 μm band is too weak to show any ODMR signals even after considerable signal averaging. The 1.5 μm band, however, shows an S = ½ resonance at $g_\perp$ = 2.07 which may result from hole centres trapped on displaced oxygen ions.

(iv) Annealing of radiation damage

The stability of the E$_1'$ centre against annealing in the temperature range 800 - 1200 K has been studied. The procedure was to allow the E$_1'$ centre concentration to decrease to its equilibrium value as a function of time after implantation. Samples were then annealed in dry N$_2$ for 5 minute intervals, quenched rapidly to 300 K after each five minute interval and E$_1'$ centre concentration measured. The results were then plotted on a semi-logarithmic scale of E$_1'$ centre concentration versus time. This established that the decay was approximately a first order process (Appendix 1). Figure 10 displays plots of the rate constant measured at each temperature as a function of the reciprocal of the absolute temperature.

$$K = \text{const} \times \exp - \left[\frac{E}{kT}\right]$$

where the constant, K, varies with implantation energy and E is an

activation energy. Apparently the pre-exponential constant is related to the initial defect concentration. The results are for P^+ ion energy of 30 keV and 120 keV: both graphs in Figure 11 have the same slope. However the decay rates at the same temperature for these different doses (e.g. 950°K) differ by a factor of 30 at these two implant energies. The value of the E is 1.8 eV.

References

1. Y. Nish, Jpn. J. App. Phys. 10, 52 (1971).

2. The early work by the ETDL group was reported in P. Caplan, E.H. Poindexter, B.E. Deal and R.R. Razouk, J. Appl. Phys. 50, 587 (1979); 52, 879 (1981). See also P. Caplan and E.H. Poindexter, J. Appl. Phys. 52, 522 (1981). There have been many other subsequent publications.

3. P.M. Lenehan and P.V. Dressendorfer, J. Appl. Phys. 54, 1457 (1983).

4. K. Brower, Phys. Rev. Lett. (1984).

5. The early measurements of SDP were reported in B. Henderson, App. Phys. Lett. 44, 230 (1984).

APPENDIX 1

Reaction Kinetics

In general the rate of a chemical reaction is proportional to the concentration of the reacting substances. The annealing of irradiation damage can be a complex process, involving vacancy/interstitial recombination, vacancy aggregation and other higher order processes. We assume since no other centres are produced; from the decay of the ESR spectra it would apear that every E_1' centre is annihilated by an interstitial so recreating the undisturbed lattice; i.e. a reaction of the form

$$E_1' + I \rightarrow SiO_2$$
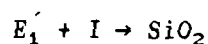
We measure the concentration of E_1' centres, C: if this decay follows a first order process the rate equation is

$$-\frac{dc}{dt} = Kc$$

where K is the rate constant. If the initial concentration is C_0, and the change in concentration after time ti is C then on substitution

$$-\frac{d}{dt}(C_0-C) = K(C_0-C)$$

so that

$$\frac{dc}{dt} = K(C_0-C)$$

By integration we find

$$\frac{C_0-C}{C_0} = \exp Kt$$

The rate constant is

$$K = \frac{1}{t} \, \ell n \left[\frac{C_0}{C_0 - C} \right] \qquad (A1)$$

Data for annealing at 950°K, given in Figure 4, shows a linear relationship between $\ell n(C_0-C)$ and the time t with rate constant $K = -0.1975 \pm (12) cm^{-1}$. The temperature dependence of K is expressed by means of the Arrhenius equation

$$K = K_0 \, \exp \left[- \frac{E}{kT} \right] \qquad (A2)$$

where K_0 is a frequency factor and E is activation energy of the reaction, which may be determined from

$$\log \left[\frac{K_1}{K_2} \right] = \frac{E}{2.303k} \left[\frac{1}{T_2} - \frac{1}{T_1} \right] \qquad (A3)$$

Data shown in Figure 11 show good agreement with eqns. 2 and 3.

Figure 1 *Showing the ESR spectrum of a Si/SiO$_2$ sample after (a) removing the SiO$_2$ layer by etching and (b) after removing the polysilicon layer also by etching. Measurement at X-band and T = 300 K.*

Figure 2 *(a) the SDP resonance in Si/SiO$_2$ measured at 24 GHz and T = 1.6 K, (b) ODMR spectrum measured coincidentally with the SDP spectrum in (a) by detecting the microwave-induced changes in the intensity of the luminescence spectrum shown in (c).*

Figure 3 *The luminescence excited by the SiO$_2$ layer on an n-type Si/SiO$_2$ wafer excited using U.V. excitation from Kr$^+$ ion laser. For comparison the spectrum excited by X-irradiation of single crystal quartz is also shown.*

Figure 4 *The ODMR spectrum of triplet excitons in the amorphous SiO$_2$ layer on an Si/SiO$_2$ wafer measured by detecting the luminescence shown in Figure 3. Recorded at 24 GHz and 1.6 K.*

Figure 5 *The ODMR spectrum of X-ray excited luminescence from SiO$_2$ layers on ⟨111⟩ surface of Si measured at $V \simeq 35$ GHz and 1.6K. The spectrum shows the change in the total light emitted in the blue emission centred at 400 nm, when $M_S = 0 \rightarrow \pm 1$ transitions are induced by resonant microwaves.*

Figure 6 *ESR spectra measured at low power of Si/SiO$_2$ wafers in which (a) 10^{13}, (b) 5×10^{14} and (c) 5×10^{15} P ions with 20 keV energy have been implanted.*

Figure 7 *The concentration of E_1' centres in the amorphous SiO$_2$ layer of Si/SiO$_2$ wafers plotted as a function of dose of implanted P$^+$ ions in various doses.*

Figure 8 *ESR spectra of Si/SiO$_2$ wafers implanted with P$^+$ ions (a) 7 days after implantation and (b) 90 days after implantation.*

Figure 9 *Showing the dose and energy dependence of E_1' centre concentration decrease with time following implantation.*

Figure 10 *Luminescence from ion implanted SiO$_2$ on ⟨111⟩ Si surfaces excited by 337 nm light from an Ar$^+$ laser. T = 77K.*

Figure 11 *Showing that the decrease in concentration of E_1' centres on annealing follows first order reaction kinetics.*

computer simulation

P_{am} - amorphous Si signal

2.0055   1.999

g - value
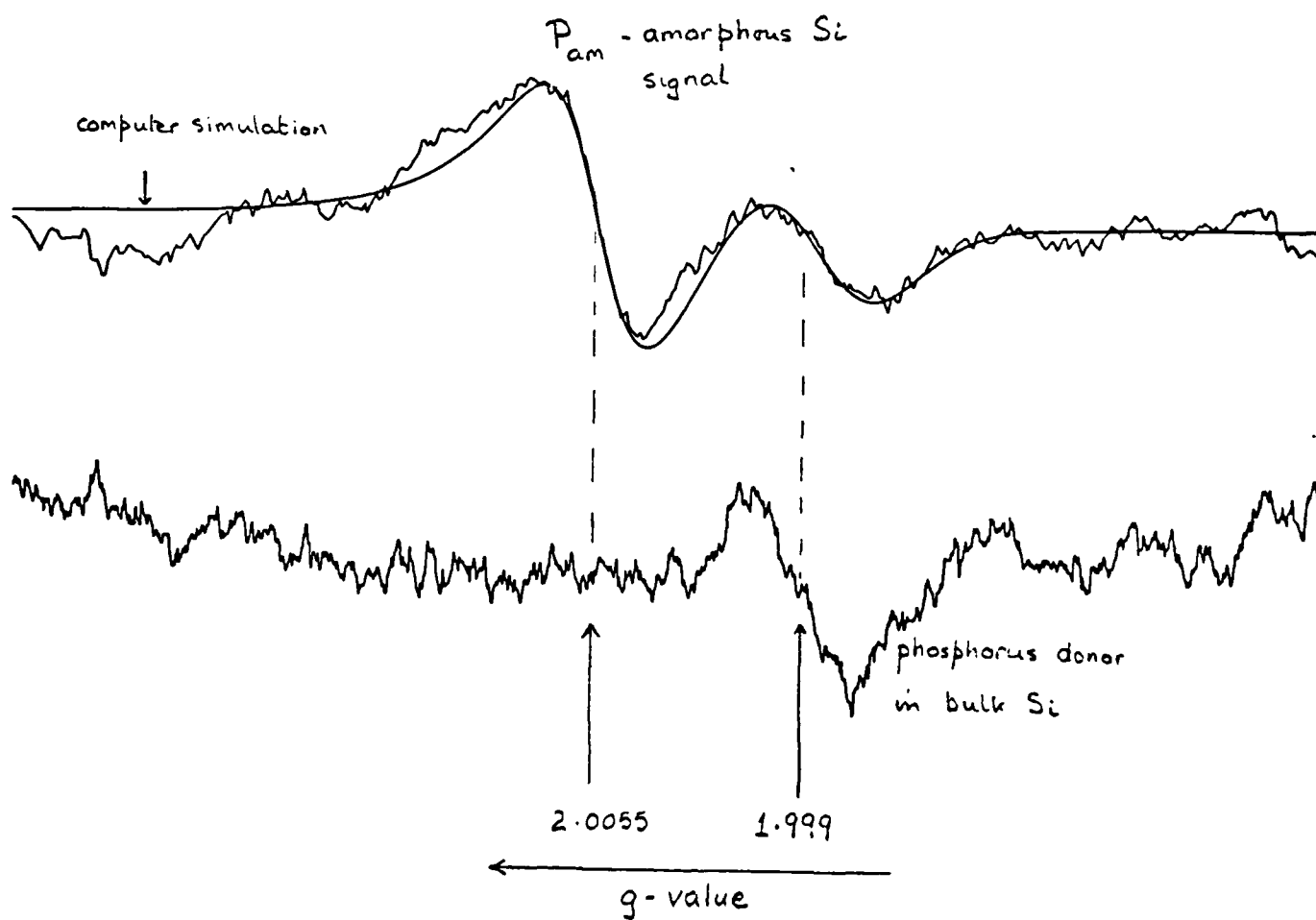
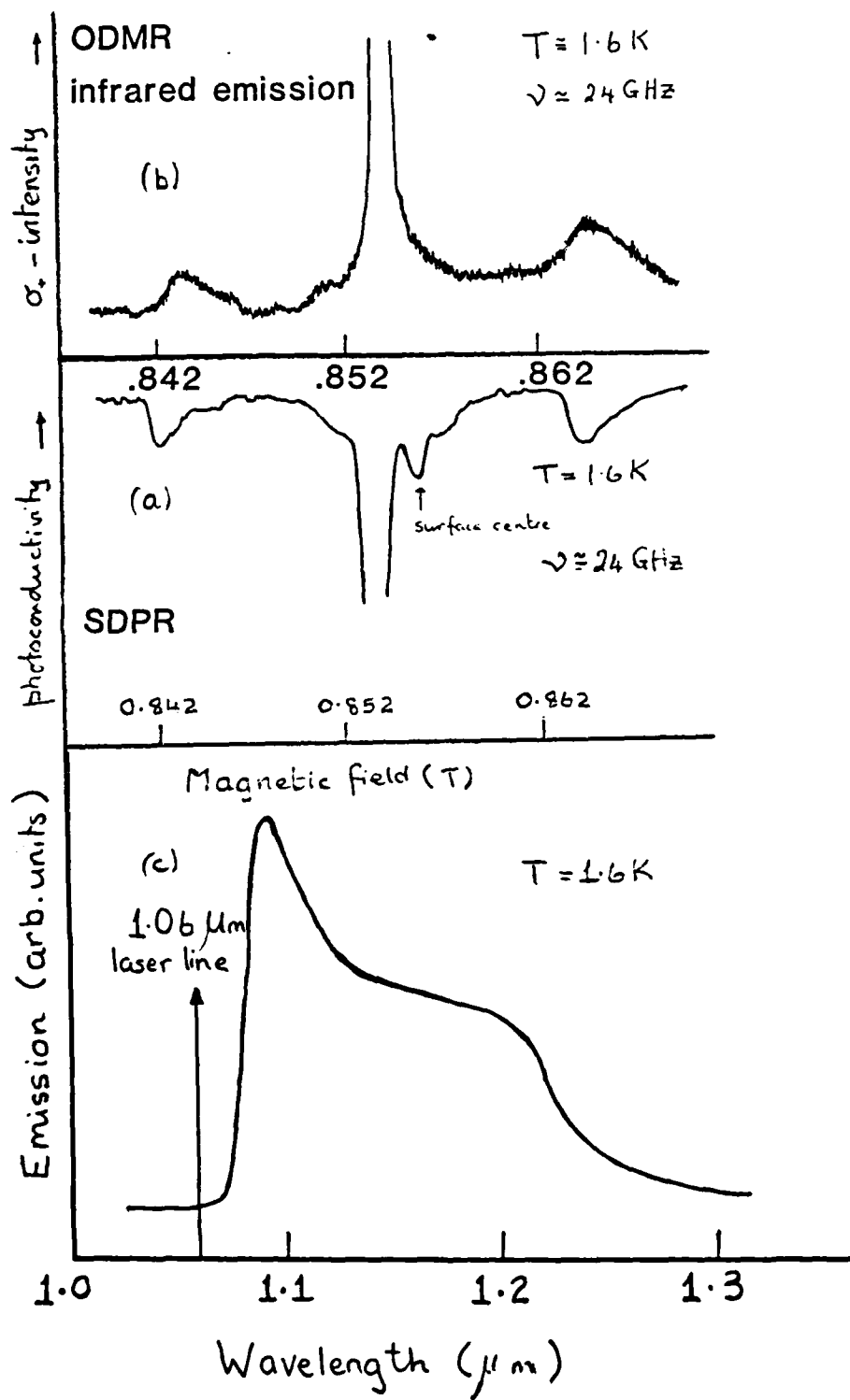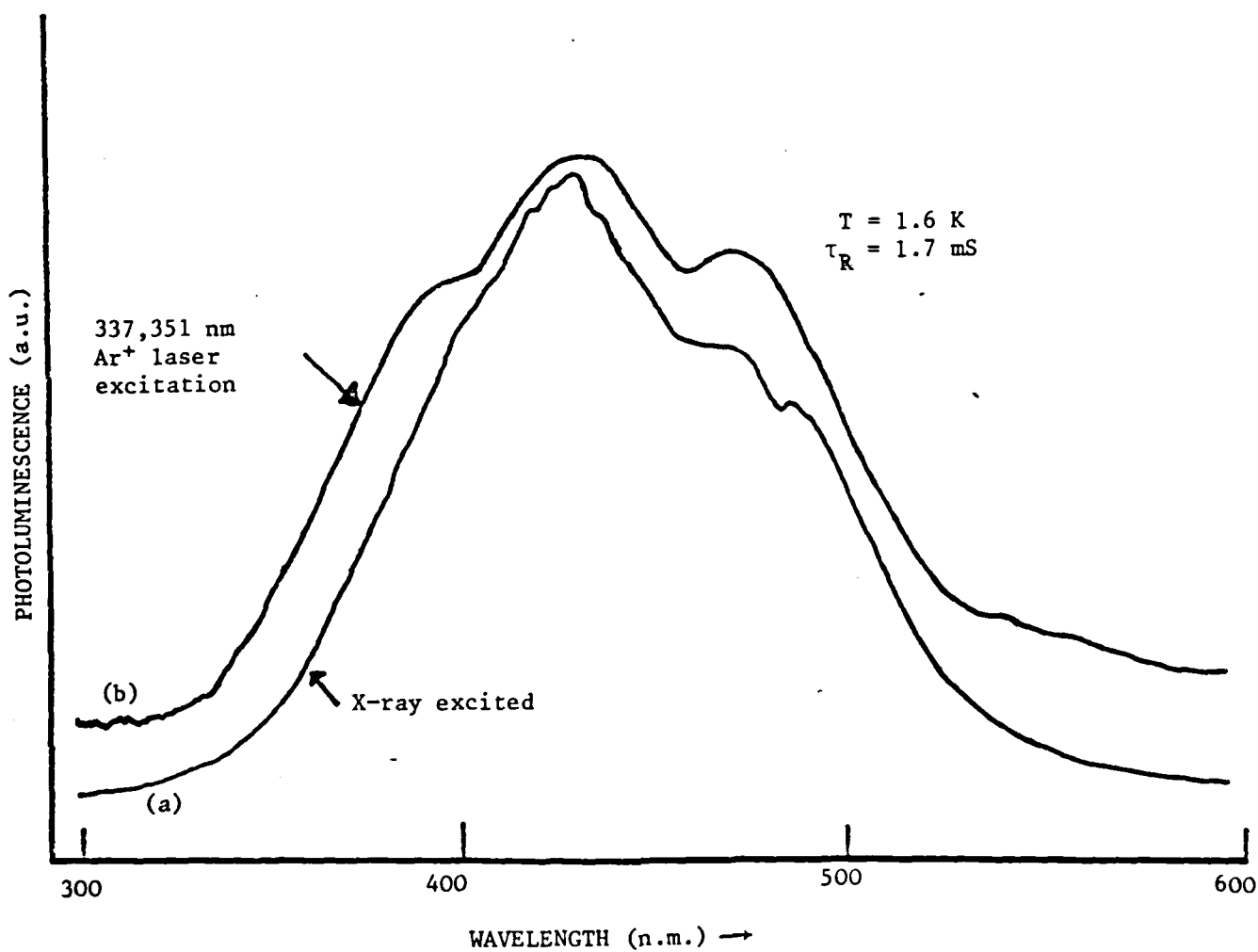phosphorus donor in bulk Si

Figure 1

Final Research Report

Figure 2

(a) SiO$_2$ single crystal (after Hayes et al. 1984).
(b) SiO$_2$ on Si (this work) - SiO$_2$ layer 200nm thickness
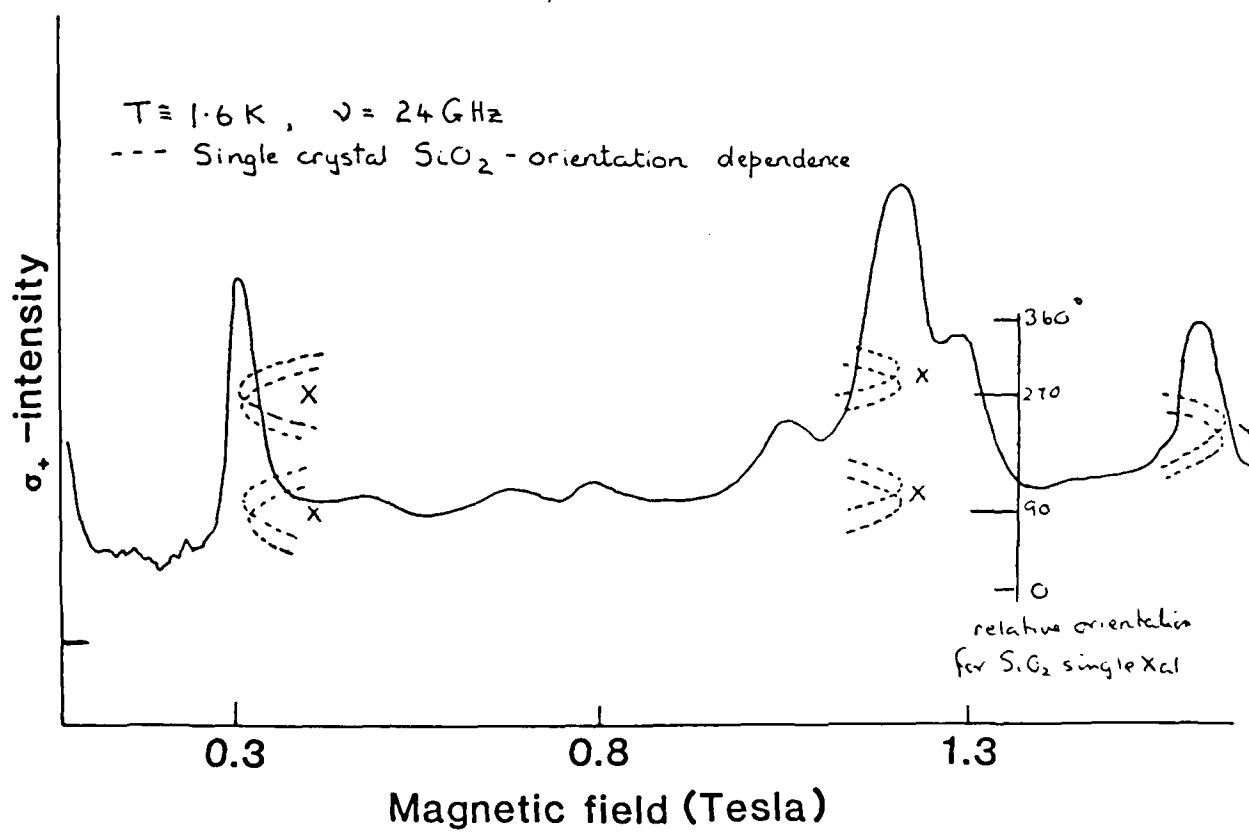
Figure 3

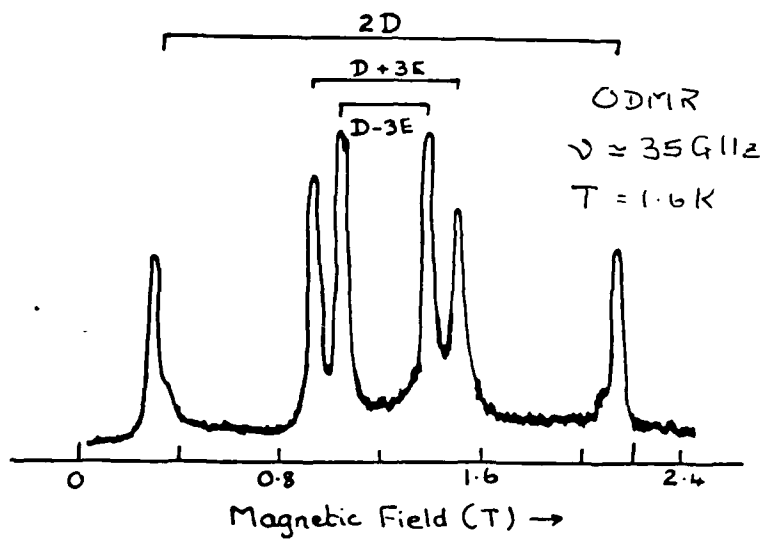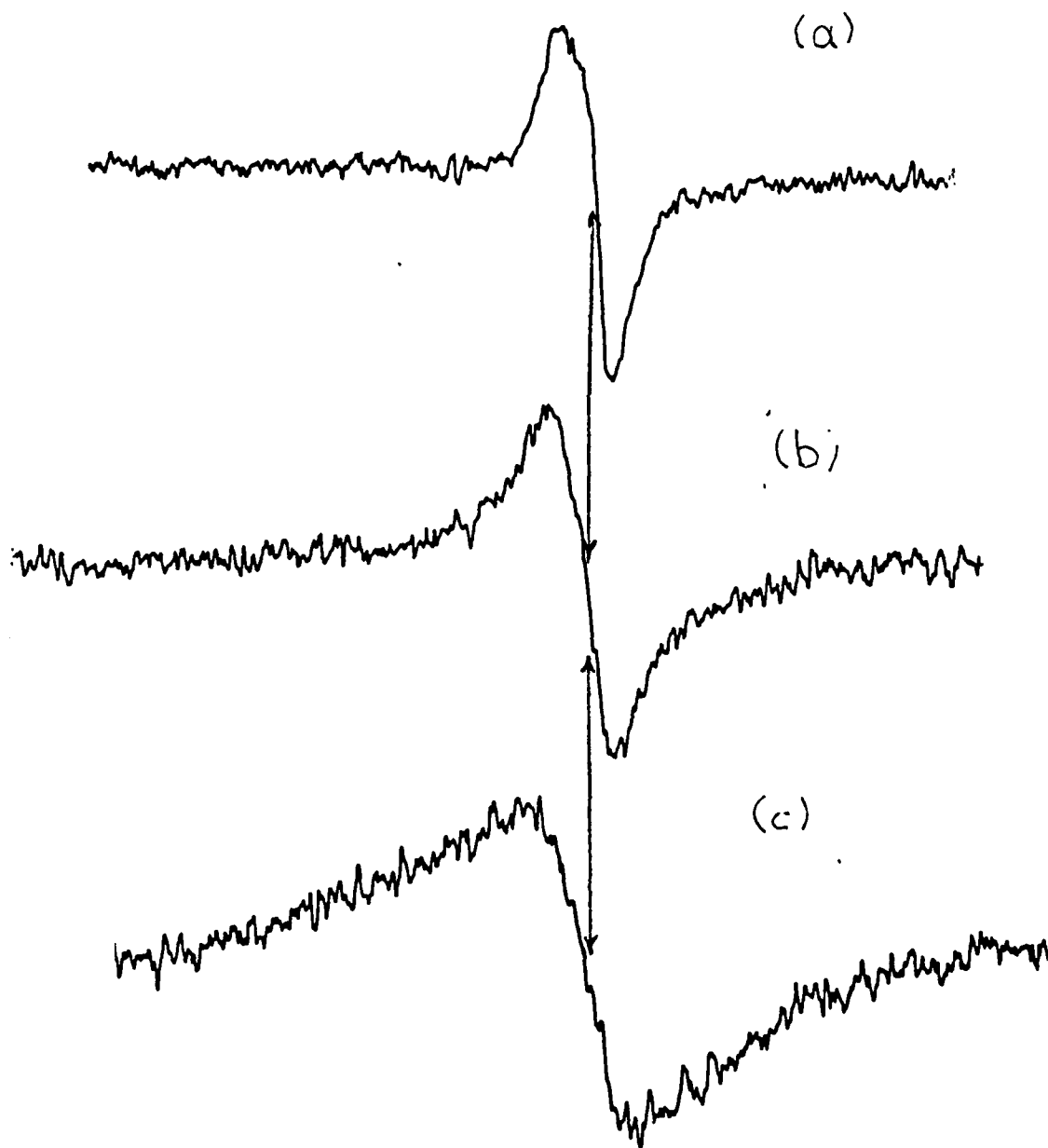Final Research Report

Figure 4

Final Research Report

Figure 5

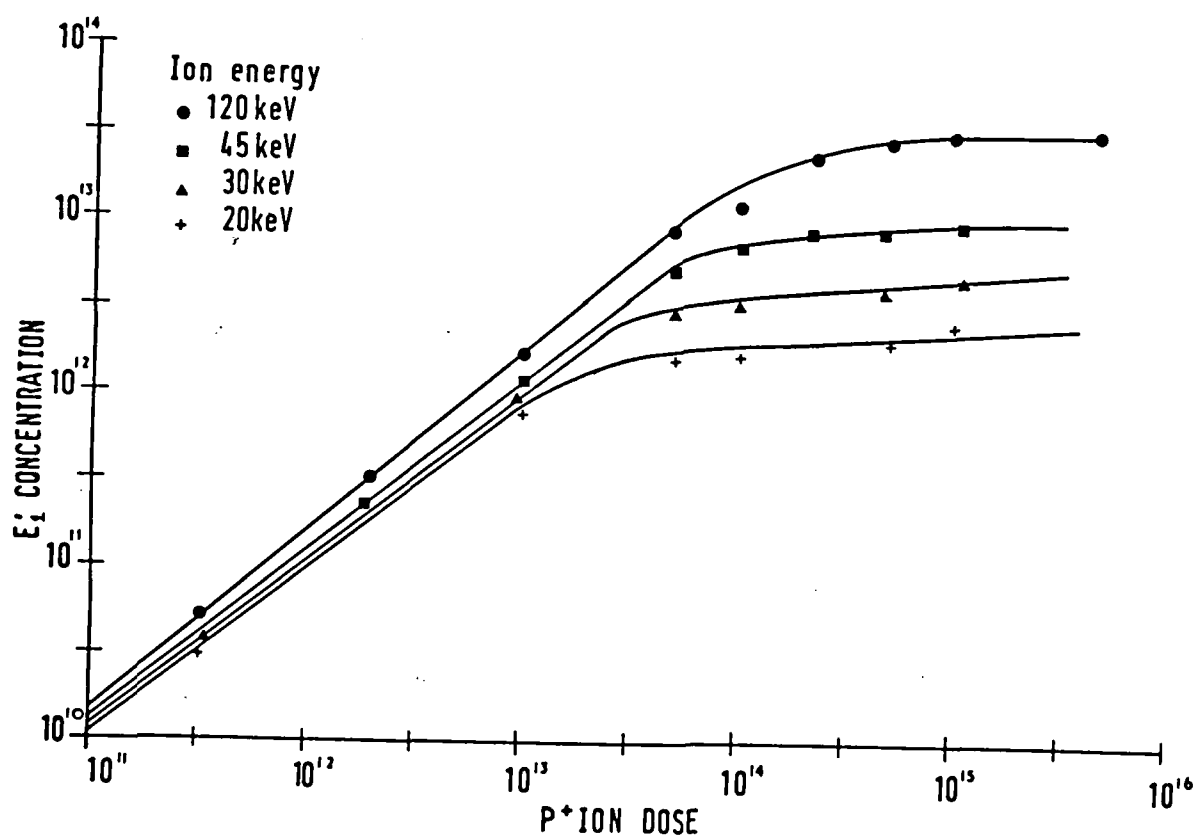Final Research Report

Figure 6

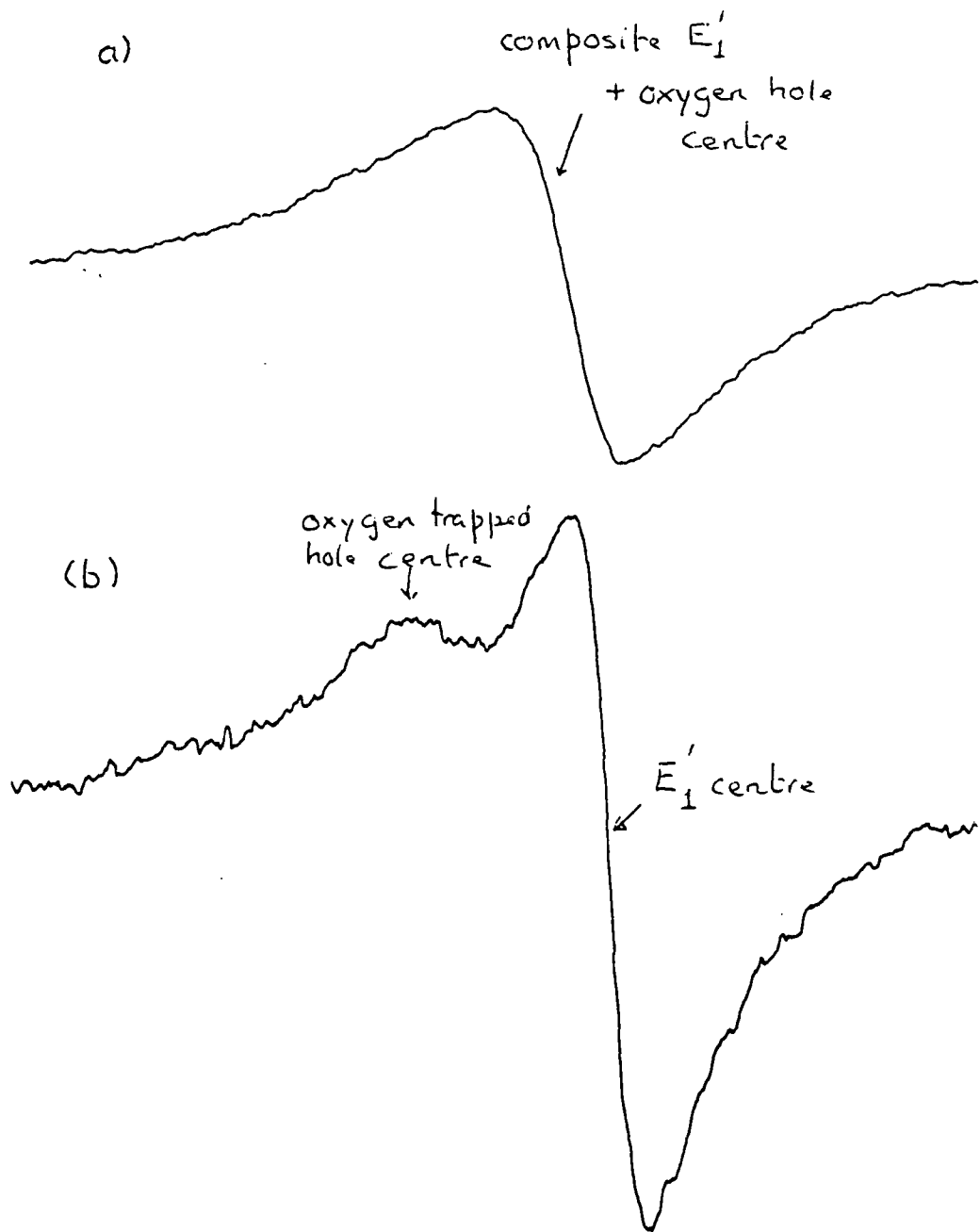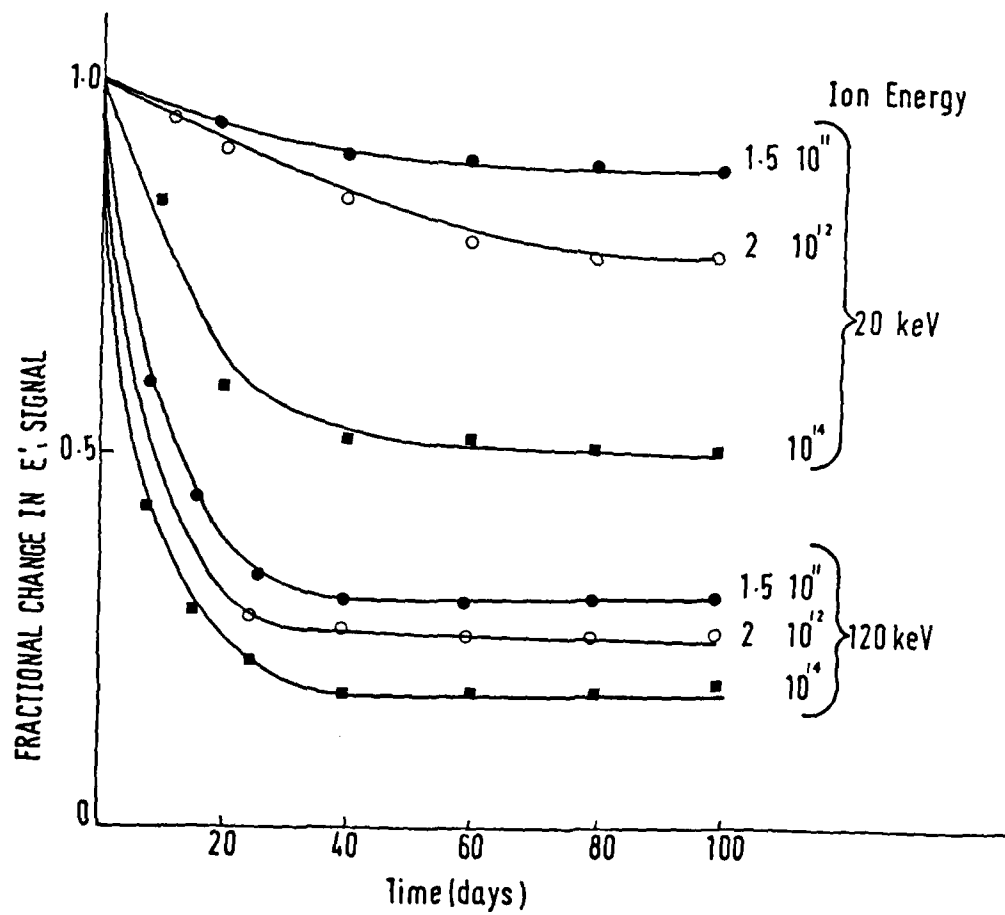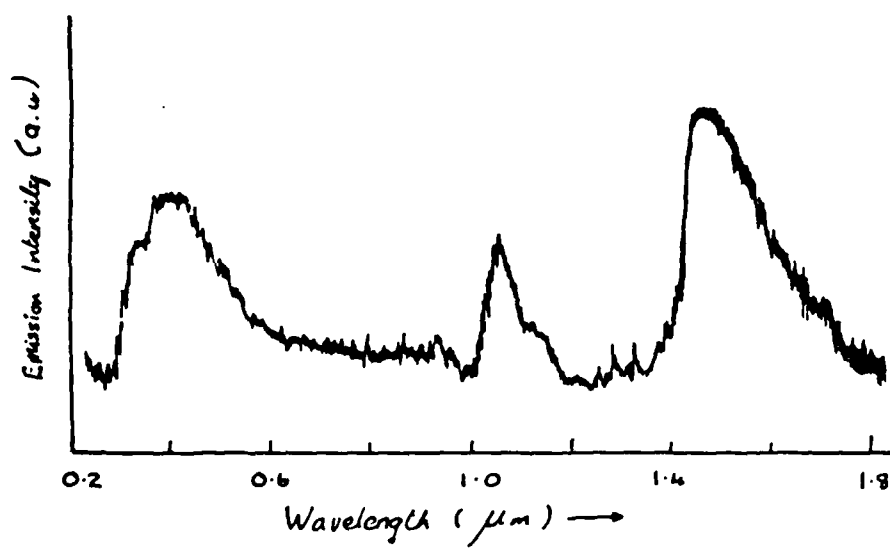Final Research Report

Figure 7

Final Research Report

a)

composite E_1'
+ oxygen hole
centre

(b)

oxygen trapped
hole centre

E_1' centre

Figure 8

Final Research Report

Figure 9
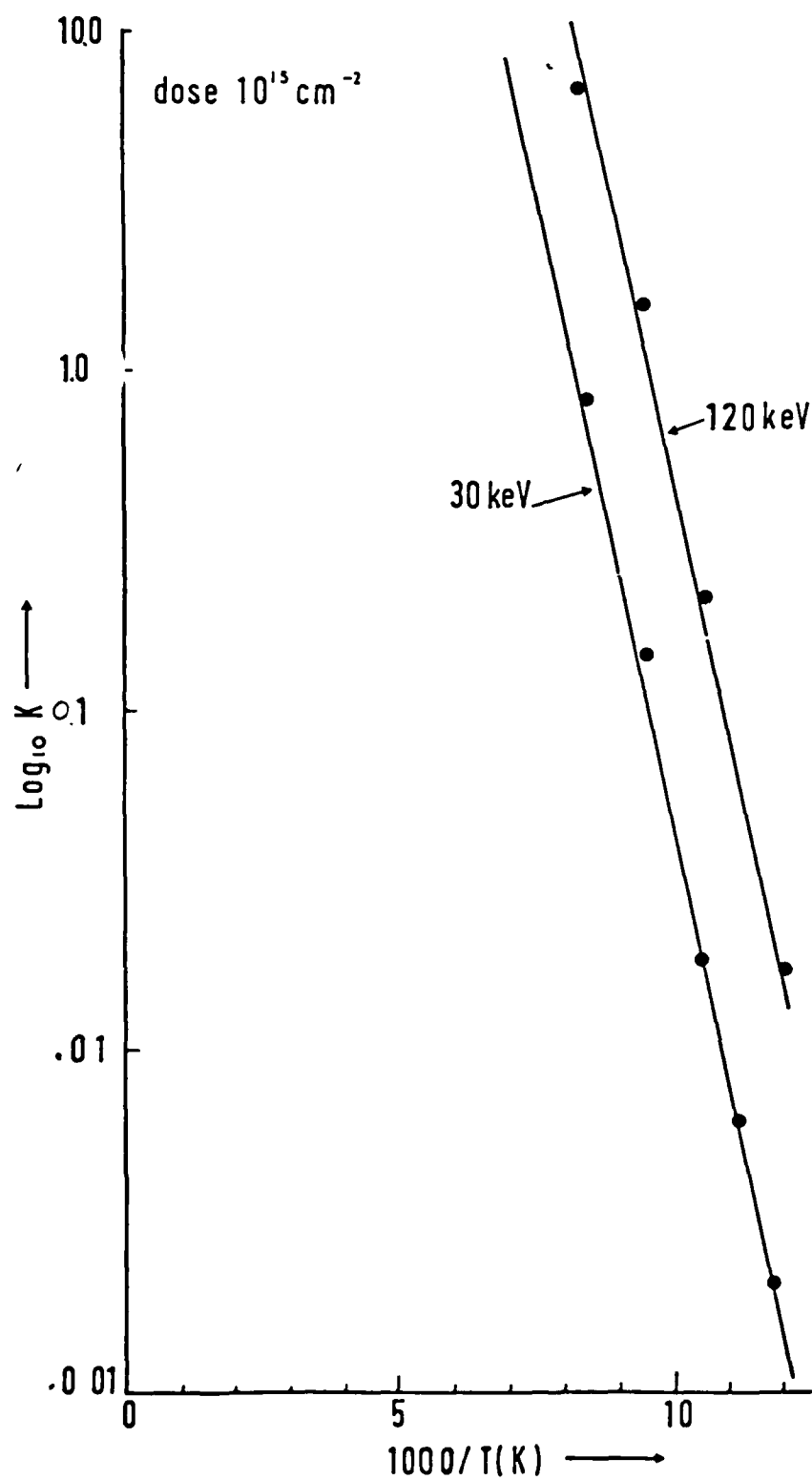
Final Research Report

Figure 10

Final Research Report

Figure 11

END

1/2 - 86

DITIC